





Ho:YLF amplifier with Ti:Sapphire frontend for pumping mid-infrared optical parametric amplifier

Cite as: Appl. Phys. Lett. **117**, 141102 (2020); <https://doi.org/10.1063/5.0021438>

Submitted: 10 July 2020 . Accepted: 10 September 2020 . Published Online: 05 October 2020

 Krishna Murari,  Fangjie Zhou, Yanchun Yin, Yi Wu, Bruce Weaver, Timur Avni,  Esben Larsen, and  Zenghu Chang



View Online



Export Citation



CrossMark

ARTICLES YOU MAY BE INTERESTED IN

[Forward and backward stimulated Brillouin scattering in aqueous suspension of SiO₂ spherical nanoparticles](#)

Applied Physics Letters **117**, 141101 (2020); <https://doi.org/10.1063/5.0024816>

[Recent twists in twisted light: A Perspective on optical vortices from dielectric metasurfaces](#)

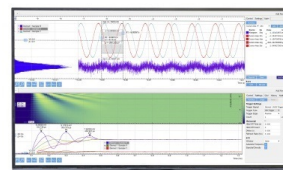
Applied Physics Letters **117**, 140501 (2020); <https://doi.org/10.1063/5.0023338>

[Trapping of multiple H atoms at the Ga\(1\) vacancy in \$\beta\$ -Ga₂O₃](#)

Applied Physics Letters **117**, 142101 (2020); <https://doi.org/10.1063/5.0024269>

Challenge us.

What are your needs for periodic signal detection?



Zurich Instruments

Ho:YLF amplifier with Ti:Sapphire frontend for pumping mid-infrared optical parametric amplifier

Cite as: Appl. Phys. Lett. **117**, 141102 (2020); doi: [10.1063/5.0021438](https://doi.org/10.1063/5.0021438)

Submitted: 10 July 2020 · Accepted: 10 September 2020 ·

Published Online: 5 October 2020











View Online



Export Citation



CrossMark

Krishna Murari,^{1,a)}  Fangjie Zhou,¹  Yanchun Yin,¹  Yi Wu,¹  Bruce Weaver,²  Timur Avni,²  Esben Larsen,²  and Zenghu Chang¹ 

AFFILIATIONS

¹Institute for the Frontier of Attosecond Science and Technology, The College of Optics and Photonics (CREOL) and Department of Physics, University of Central Florida, Orlando, Florida 32816, USA

²Quantum Optics and Laser Science Group, Blackett Laboratory, Imperial College London, London SW7 2BW, United Kingdom

^{a)} Author to whom correspondence should be addressed: krishnacelos@gmail.com

ABSTRACT

We present a Ho:YLF Chirped-Pulse Amplification laser for pumping a longwave infrared Optical Parametric Chirped Pulse Amplifier at a 1 kHz repetition rate. By utilizing a Ti:Sapphire laser as a frontend, 5- μ J seed pulses at 2051 nm laser pulse are generated in a Dual-Chirp Optical Parametric Amplifier, which are amplified to 28 mJ pulses with a pulse duration of 5.6 ps. The scheme offers a potential driver for two-color (800 nm and 8 μ m) high harmonic generation with an increased keV x-ray photon flux.

Published under license by AIP Publishing. <https://doi.org/10.1063/5.0021438>

Ultrashort intense mid-wave-infrared (MWIR) and long-wave-infrared (LWIR) laser pulses are of great importance to strong-field physics and attosecond science experiments. Recent development of carrier-envelope phase (CEP)-stabilized few-cycle lasers at a wavelength of 1.6–2.1 μ m has paved the way for the next generation of attosecond light sources with photon energies reaching the water window (284 eV–530 eV).^{1,2} Scaling of photon energies by high-order harmonic generation (HHG) to a few keV requires the development of high-energy few-cycle pulses extending into the LWIR wavelength because the cut-off photon energy of the HHG process scales quadratically with the driving laser wavelength. Furthermore, LWIR lasers are an ideal tool to study HHG in solids,³ acceleration of electrons in dielectric structures and plasma,⁴ breakdown of the dipole approximation,⁵ and rotational/vibrational spectroscopy.⁶ X-rays at 1.6 keV have been produced using lasers at 3.9 μ m.⁷ However, the conversion efficiency decreases with the increasing wavelength of the driving laser,⁸ thereby reducing the total flux of the attosecond pulses. To be able to perform time-resolved pump-probe experiments such as transient absorption spectroscopy and attosecond streaking, innovative schemes are needed to enhance the attosecond photon flux when driven with LWIR lasers. In this context, multi-color laser fields have been suggested to increase the harmonic yield and extend the cut-off energy.⁹ For instance, when the HHG process is driven by two-color fields (a

strong infrared field and a weak attosecond extreme ultraviolet), the harmonic yield can be enhanced.¹⁰ In the case of keV x-rays driven by a single-cycle LWIR laser centered at 8 μ m, it has been predicted theoretically that the intensity of an x-ray pulse can be significantly enhanced by adding a few times weaker few-cycles near the infrared pulse centered at \sim 800 nm.¹¹ As described in Ref. 11, the variation of the CEP of the 8 μ m pulses should be less than 0.27 rad, whereas the CEP jitter of the 800 nm pulse should be less than 0.04 rad. It is a grant technique challenge to develop a laser system to deliver the two synchronized pulses with the required CEP stability.

High-energy femtosecond MWIR/LWIR pulses can be generated using an optical parametric chirp pulse amplifier or an optical parametric amplifier (OPA) involving frequency conversion in a nonlinear medium. Most lasers developed so far in this regime are limited to wavelengths up to 3–4 μ m due to the oxide-based nonlinear crystals used, which have limited transparency beyond this wavelength. Extending the wavelength further into the LWIR requires the frequency conversion in a non-oxide crystal like zinc germanium phosphide (ZGP). However, such a crystal is not transparent below 1.9 μ m, therefore pumping the OPA at longer wavelengths than provided by ytterbium (\sim 1.03 μ m) and neodymium (\sim 1.06 μ m) doped YAG lasers is required. Hence, the development of high-energy longer wavelength ($>$ 1.9 μ m) pump sources becomes crucial in the generation of high

peak power LWIR pulses. In recent years, several studies have been published in this regard generating a wide range of pulse energies in the $2\text{-}\mu\text{m}$ wavelength range based on a rare earth Ho^{+3} (holmium) ion doped gain medium.^{12–15} In this regard, most of the $2\text{-}\mu\text{m}$ high energy lasers are based on Ho:YLF or Ho:YAG developed so far. A Ho:YAG based multi-millijoule regenerative amplifier (RA) was first demonstrated by Malevich *et al.*¹⁶ By pumping the system using a Tm-based fiber laser and Yb-laser based OPA as a seed, they generated 3 mJ pulses at a repetition rate of 5 kHz. Hemmer *et al.* demonstrated Ho:YLF based RA at 100 Hz producing pulses at 5.5 mJ, which was further amplified to 39 mJ in cryogenically cooled booster amplifier with a bandwidth of only $\sim 1.3\text{ nm}$. Murari *et al.* demonstrated Ho:YLF RA at 1 kHz at a lower energy of 2.2 mJ, but by employing an intracavity filter inside the RA cavity, they enhanced the spectral bandwidth to $\sim 5\text{ nm}$. Kroetz *et al.* operated RA in a new regime emitting pulses at 1 kHz and an energy of 6.9 mJ. Grafenstein *et al.* utilized a Ho:YLF based RA to reach 10 mJ, which was then amplified in two-stage booster linear amplifiers to reach an energy up to 55 mJ. In this case, an amplified gain of 10^8 was achieved owing to the typical damage threshold of the Ho:YLF crystal of 16 GW/cm^2 . The high gain in the system leads to a long output pulse duration owing to gain narrowing. Nevertheless, by utilizing this system, an Optical Parametric Chirped Pulse Amplifier (OPCPA) emitting 1 mJ, 100 fs pulses at $5.1\text{ }\mu\text{m}$ has been demonstrated.¹⁷ Very recently, Grafenstein *et al.* demonstrated an improved amplifier system emitting pulses of energy 52 mJ and a duration of 2.4 ps.¹⁸ However, in order to use this system to generate a sufficient HHG yield for pump probe experiments, as mentioned before, it would be beneficial to add a second near-infrared pulse at, for example, $\sim 800\text{ nm}$ for a two-color HHG scheme. Such experiments require an mJ-level single-cycle pulse at both wavelengths with CEP stability. The CEP stability becomes a challenge if the Ho:YLF pump laser is seeded by a different laser as that of the seed generated for the LWIR OPCPA. Hence, in order to perform two-color HHG, it is advantageous to use a Ti:Sapphire as a front-end which can serve as a seed for threefold purpose; first, to generate narrowband μJ -level $2.05\text{ }\mu\text{m}$ pulses for seeding a Ho:YLF amplifier through dual-chirp OPA;¹⁹ second, to generate a CEP stable seed for the broadband LWIR OPCPA through hollow-core fiber broadening and intrapulse difference frequency generation (IDFG);²⁰ and third, utilizing the phase-stable high-energy idler of the LWIR OPCPA added to the low-energy near-infrared pulse for the two-color HHG thereby enabling enhanced HHG yield.¹¹ Since the entire system is driven by a single Ti:Sapphire laser system as a frontend, the final output pulse can be CEP stabilized. Figure 1 shows the schematic of our proposed two-color HHG scheme. Figure 2 shows the schematic of the $2\text{-}\mu\text{m}$ pulse generation with the Ti:Sapphire laser as frontend.

Here, we report on a multi-stage Ho:YLF based amplifier at a 1 kHz repetition rate and picosecond pulse duration. We demonstrate the amplification of μJ -level pulses to 36 mJ in a four stage amplifier with continuous-wave (CW) pumping at an extraction efficiency of $\sim 14\%$. The Ho:YLF crystals are end-pumped using three commercial CW Tm-fiber lasers from IPG Photonics, Inc. The amplifier employs a conventional chirped pulse amplification scheme. A single reflection-based Chirp Volume Bragg Grating (CVBG) is used for both stretching and compression of the pulses, which significantly reduces the overall system footprint as compared with a system that utilizes diffraction gratings.¹⁴ Deploying multiple amplification stages allows us

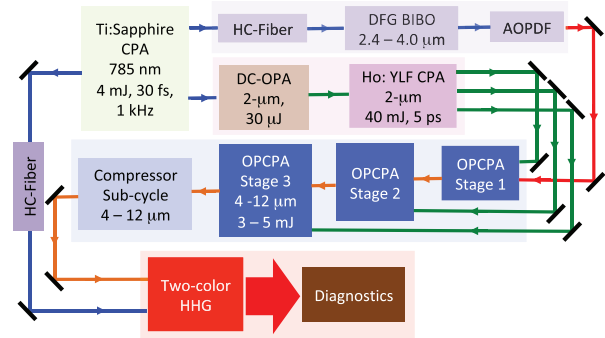


FIG. 1. Schematic of the two-color HHG driven by LWIR with the Ti:Sapphire laser as frontend.

to easily optimize the spot size of the seed beam independently in the different gain crystals. The laser system is maintained at room temperature, while the crystals are water-cooled to $18\text{ }^\circ\text{C}$ and is purged with dry nitrogen to a humidity level of $<1\%$.

The seed source consists of a 14-pass Ti:Sapphire amplifier pumped Dual-Chirp Optical Parametric Amplifier (DC-OPA) based on the Beta Barium Borate (BBO) crystal. The Ti:Sapphire amplifier emits pulses at 30 fs and 4 mJ at 1 kHz repetition rate centered at 785 nm. Only 1 mJ pulse is used to pump the DC-OPA, which is divided into two beams using a 1% transmission and 99% reflection beam splitter. The weaker of the two beams is focused in a 3 mm YAG window to generate broadband white light. The white light is then positively chirped before being used to seed a single-stage BBO based collinear OPA, which is pumped by the remaining of 0.99 mJ. The OPA generates $36\text{ }\mu\text{J}$ idler pulses at 2051 nm and its measured Gaussian beam profile is shown in Fig. 3, whose M^2 values in the x and y directions are 2.1 and 2.4, respectively. The details of the OPA can be found here.¹⁹ The idler pulse at 2051 nm is chosen to match the gain bandwidth of the Ho:YLF crystal and has a full-width at half-maxima (FWHM) bandwidth of 20 nm. However, due to the limited reflection bandwidth of the CVBG in the stretcher, the idler spectrum bandwidth is further reduced to $\sim 4.5\text{ nm}$ leading to a pulse energy of $2\text{ }\mu\text{J}$. It must be noted here that it is not advantageous to seed the amplifier with a broader spectrum as the narrow gain bandwidth of the Ho:YLF crystal will lead to a narrowed spectrum after amplification. Figure 3 shows the schematic design of the multi-stage amplifier. The seed pulses are incident normally on the CVBG from the red-to-blue side in the forward direction through the polarization-rotation scheme that utilizes a thin-film polarizer (TFP) and a quarter waveplate (QWP). The seed

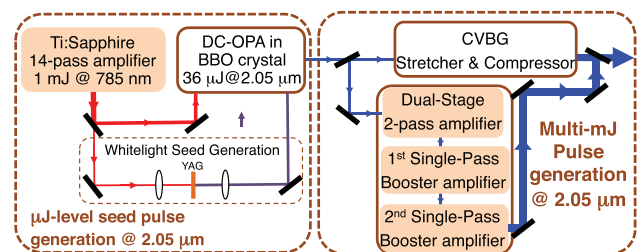


FIG. 2. Schematic of the $2\text{-}\mu\text{m}$ pulse generation.

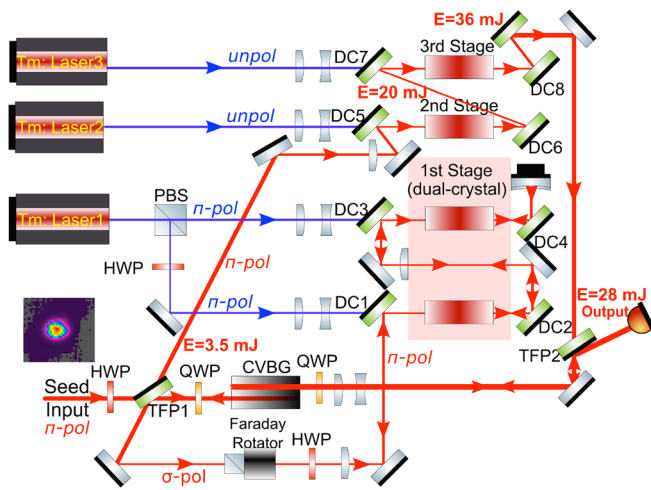


FIG. 3. Experimental layout of the amplifier system.

beam is stretched to a pulse duration of 490 ps and is reflected backwards. The stretched beam is reflected off the same TFP due to the rotation from π - to σ -polarization, which is then injected into the first stage, two-crystal, two-pass amplifier. Before injection, the beam is passed through a Faraday Rotator (FR) with a clear aperture of 4 mm. The FR rotates the incoming σ -polarized seed beam by 45° in the forward direction and the half-wave plate (HWP) is placed such that it further rotates the polarization by 45° , thereby converting the seed beam from σ - to π - polarization and is seeded in the first stage, two-crystal, two-pass amplifier.

The crystals are 50 mm long, a-cut, 0.75% doped Ho:YLF cylindrical rods with clear apertures of 5 mm diameter. The rods are mounted on indium-contacted copper holders that are water-cooled to 18°C . The crystals are pumped using a single Tm-fiber laser that emits unpolarized CW 1940 nm light with a power of 120 W. The absorption cross sections of the pump for polarizations perpendicular and parallel to the c -axis are $0.58 \times 10^{-20} \text{ cm}^2$ and $1 \times 10^{-20} \text{ cm}^2$, respectively, while the emission cross sections at 2051 nm are $0.78 \times 10^{-20} \text{ cm}^2$ and $1.5 \times 10^{-20} \text{ cm}^2$, respectively. Hence, to achieve maximum gain, the polarizations of both the pump and the seed beams are parallel to the crystal c -axis. The optical axis of the crystal is aligned by rotating the crystal with the incident pump beam and optimized for maximum absorption before it is mounted in the copper holder. The pump absorption in the crystal is 99%. The CW output of the Tm-fiber laser is first split into two equal σ - and π -polarized beams using an optically contacted polarizing beam splitter (PBS) cube leading to 60 W of maximum pump power in each arm of the PBS. In the co-linear geometry, the π -polarized transmitted beam through the PBS is sent to the second crystal of the first stage amplifier, while the σ -polarized reflected beam from the PBS is then converted to π -polarization by passing through a HWP and then sent into the first crystal of the first stage amplifier through dichroic mirror DC1 that is highly reflective at 2051 nm and transmits at 1940 nm. The dichroic mirrors are custom dielectrics coated to reflect $>99\%$ at 2050 nm for the seed beam while transmitting $>98\%$ at 1940 nm of the pump beam. The pump is tightly focused to a beam diameter ($1/e^2$) of 0.7 mm and mode matched in the crystal with the seed using a

telescope with a convex and a concave lens combination. The stretched seed pulses are combined with the pump beam using the DC1 and focused into the first crystal of the first stage amplifier using a lens of focal length 400 mm to a beam diameter of 0.7 mm as shown in Fig. 3. After amplification of the seed pulse in the first crystal, the unabsorbed pump is separated using another dichroic mirror DC2. The unabsorbed pump power is separated and then dumped out of the system using another dichroic mirror DC2, while the amplified pulse is sent to the second crystal of the first stage amplifier with the same parameters and design geometry as that of the first crystal. The remaining pump can potentially be reused in the double-sided pump geometry to improve the amplifier optical efficiency of the system.

After amplification of the seed beam in the first pass of the first stage amplifier in the two crystals, the seed is then refocused back into the two-crystal of the first stage amplifier using a concave mirror. Since the back reflected beam passes again through the first crystal of the first stage, the radius of curvature of the concave mirror is precisely chosen to keep the seed spot size in the first crystal (second pass) below the damage threshold of the crystal. After the amplification in the two-crystal of the first stage, the amplified pulse re-encounters the HWP and FR. However, in the reverse direction due to the directional property of the FR, the effect of HWP is reversed and the exiting pulse remains π -polarized. The π -polarized amplified beam is transmitted through the TFP thereby exiting the dual-crystal first stage amplifier. Thus, the amplified pulse with an energy of 3.5 mJ from the first stage is ejected out of the amplifier using the four-way port of the TFP. The total pump power used in the first stage is 28 W (out of the total available power of 120 W). The pulse is subsequently amplified into two single-pass (second and third stage) booster amplifiers. The seed fluence in each stage is chosen by adjusting the spot size to avoid damage of the anti-reflection (AR) coating of the crystals.

The second stage amplifier is aligned similar to the first stage. However in this stage, the seed pulse passes through the gain medium just once. The crystal length is 50 mm. The pump and seed beam diameters are maintained at 1.5 mm. The pump power is derived from a second Tm-fiber laser with a total unpolarized pump power of 120 W. Both the pump and seed beams are aligned collinearly into the gain medium through the dichroic mirror DC5. However, in order to operate the dichroic mirror DC5 for both the unpolarized pump beam at 1940 nm with transmission $>98\%$ and the π -polarized seed beam at 2051 nm with reflection $>99\%$, the dielectric coating on dichroic mirror DC5 is redesigned for an incident angle (AOI) $<20^\circ$ contrary to that used in the first stage with AOI at 45° . After amplification the amplified seed and the unabsorbed pump beams are again separated using a second dichroic mirror DC6. The unabsorbed pump beam in the Ho:YLF crystal of the second stage is transmitted out of the system to beam dump, while the amplified beam is sent into the third stage. The 3.5-mJ pulses from the first stage are amplified to 20 mJ in the second stage pumped by an unpolarized pump power of 120 W. Figure 4 shows the output energy from the first and second stage amplifier plotted against the pump power.

Finally, the output of the second stage seeds the third stage for further amplification through DC8. The third stage amplifier is also pumped by an unpolarized beam of 130 W derived from a third Tm-fiber laser. In the third stage, the pump and seed beams counter-propagate in the crystal, contrary to that in the first and second stage where the pump and seed beams propagate both in the same direction.

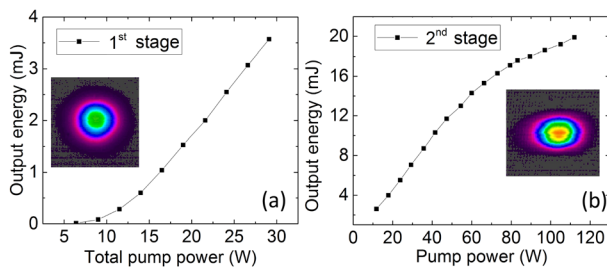


FIG. 4. Output energy vs pump power: (a) first stage output energy and (b) second stage output energy. In the insets are shown the corresponding beam profiles.

The dichroic mirror DC7 separates the pump and seed beams as shown in Figure 3. The pump and seed beam diameters in the third stage are chosen to be 2.2 mm to avoid laser damage. After amplification, the unabsorbed pump and the amplified seed beams are separated using DC8. Due to the lower pump absorption for the polarization perpendicular to the c -axis of the crystal, the transmitted power is high. Therefore, a water-cooled beam dump is used to reduce the heating effect on the dump. In the third stage, the 20-mJ seed pulse is further amplified to 36 mJ, although by reducing the seed beam diameter further and pumping it with higher power can permit us to increase the amplification beyond 40 mJ. However, the pulse energy was restricted to operate in the safe regime away of damage threshold of the AR coating to avoid damage. We operate the third stage at the peak intensity below 8 GW/cm^2 . Due to the higher temperature dependence of the refractive index (dn/dT) along the c -axis of the crystal, the thermal lensing effect stretches the beam profile in one direction. Therefore, the third stage crystal is rotated by 90° with respect to the second stage in order to balance the astigmatism. The polarization of the seed beam is rotated accordingly to ensure the optimum amplification. This improves the output beam profile to be more circular.

Finally, the amplified pulse is compressed using the same CVBG that was used initially for stretching. The front side of the CVBG was used to stretch the pulse from the red-to-blue side, while the backside is used to compress the pulse from the blue-to-red side. This configuration avoids any chirp mismatch arising due to possible misalignment where separate gratings are used for stretching and compression and is economical avoiding the cost of an extra pair of gratings. However, the high intensity region may suffer thermal distortions and as the seed and the amplified pulse travel different regions in the CVBG, the compressor may not compensate the chirp completely. Before sending the amplified pulses to the CVBG for compression, the pulses are sent through the similar configuration of TFP and QWP as used before in the stretcher. The amplified pulses are sent into the CVBG at normal incidence. Figure 5 shows the results obtained after amplification from the third stage. Figure 5(a) shows the output energy plot after the third stage before (black) and after compression (red) vs pump power used in the third stage. The transverse dimension of the CVBG is a $27 \times 20 \text{ mm}^2$ clear aperture and a length of 49 mm with a spectral bandwidth of 4.5 nm. The CVBG is in particular, designed to operate at a high energy by Optigrate, Inc. above a peak power of 3 GW/cm^2 and a pulse energy above 50 mJ. With the 36-mJ input on to the CVBG, the output energy is 28 mJ yielding the compression efficiency of 78%. This is the highest pulse energy ever achieved in a kHz Ho:YLF laser system utilizing CVBG as a compressor. The previous compression

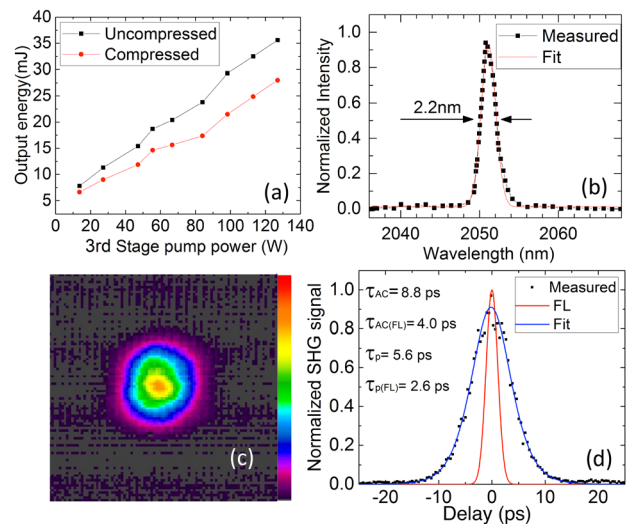


FIG. 5. Experimental results after the third stage: (a) output energy before (black) and after compression (red) vs total pump power used in all the stages, (b) output spectrum $\lambda_{FWHM} = 2.2 \text{ nm}$, (c) beam profile before compression, and (d) the autocorrelation trace with sech^2 -fitting; $\tau_{ac} = 8.8 \text{ ps}$ is the autocorrelation duration and $\tau_p = 5.6 \text{ ps}$ is the fitted pulse duration.

reported in CVBG was operated below 25 mJ to avoid the damage of the CVBG.¹⁵ In addition, our autocorrelation results show reduced energy content in the satellites. Figure 5(b) shows the output spectrum measured using a high resolution of (0.85 nm) NIRQuest spectrometer from Ocean Optics. A λ_{FWHM} of 2.2 nm of the spectrum is achieved. Figure 5(c) shows the beam profile after the third stage before compression measured using a Spiricon Pyrocam III camera. The M^2 of the output beam before the compressor in the x and y directions are 1.9 and 1.7, respectively. To characterize the temporal profile of the final amplified and compressed pulse, a commercial autocorrelator for $2 \mu\text{m}$ is used. The autocorrelation trace is shown in Fig. 5(d) with a sech^2 -fitting showing an 8.8 ps FWHM autocorrelation trace corresponding to an FWHM pulse duration (τ_p) of 5.6 ps. Compared to the results reported in Refs. 15 and 16, our pulse does not have any satellite pulse. We believe this might be due to the absence of the Pockels Cell in our design contrary to that used in their RA. In conclusion, we have developed a compact high power Ho:YLF amplifier at 1 kHz with a pulse energy $>28 \text{ mJ}$. The pulses are stretched and compressed using a single CVBG, with the output compressed to $\tau_p = 5.6 \text{ ps}$. The final output energy can be further increased by utilizing the full pump power in the first stage. The amplifier will enable the production of few-cycle LWIR pulses in an OPCPA scheme, where it will act as the pump laser.^{15,21} Finally, as the amplifier is seeded by a phase-stable Ti:Sapphire frontend, this will pave the way for two-color driven HHG utilizing NIR and LWIR pulses allowing the generation of high flux keV attosecond x-rays.

This work was funded by the U.S. Air force Office of Scientific Research (AFSOR) (Nos. FA9550-17-1-0499, FA9550-16-1-0013, and FA9550-15-1-0037), the Army Research Office (ARO) (Nos. W911NF-19-1-0224 and W911NF-14-1-0383), the Defense Advanced Research Project Agency (DARPA) (No. D18AC00011),

the Defense Threat Reduction Agency (No. HDTRA11910026), the National Science Foundation (NSF) (No. 1806575), and DSTL/EP SRC (No. MURI EP/N018680/1).

DATA AVAILABILITY

The data that support the findings of this study are available from the corresponding author upon reasonable request.

REFERENCES

- ¹X. Ren, J. Li, Y. Yin, K. Zhao, A. Chew, Y. Wang, S. Hu, Y. Cheng, E. Cunningham, Y. Wu, M. Chini, and Z. Chang, *J. Opt.* **20**, 023001 (2018).
- ²G. J. Stein, P. D. Keathley, P. Krogen, H. Liang, J. P. Siqueira, C.-L. Chang, C.-J. Lai, K.-H. Hong, G. M. Laurent, and F. X. Kärtner, *J. Phys. B* **49**, 155601 (2016).
- ³S. Ghimire, A. D. DiChiara, E. Sistrunk, P. Agostini, L. F. DiMauro, and D. A. Reis, *Nat. Phys.* **7**, 138–141 (2011).
- ⁴I. Jovanovic, G. Xu, and S. Wandel, *Phys. Procedia* **52**, 68–74 (2014).
- ⁵H. R. Reiss, *Phys. Rev. Lett.* **101**, 043002 (2008).
- ⁶S. Woutersen, U. Emmerichs, and H. J. Bakker, *Science* **278**, 658–660 (1997).
- ⁷T. Popmintchev, M.-C. Chen, D. Popmintchev, P. Arpin, S. Brown, S. Alisauskas, G. Andriukaitis, T. Balciunas, O. D. Mucke, A. Pugzlys, A. Baltuska, B. Shim, S. E. Schrauth, A. Gaeta, C. Hernandez-Garcia, L. Plaja, A. Becker, A. Jaron-Becker, M. M. Murnane, and H. C. Kapteyn, *Science* **336**, 1287–1291 (2012).
- ⁸B. Shan and Z. Chang, *Phys. Rev. A* **65**, 011804 (2001).
- ⁹G. Orlando, P. P. Corso, E. Fiordilino, and F. Persico, *J. Phys. B Mol. Opt. Phys.* **43**, 025602 (2010).
- ¹⁰M. B. Gaarde, K. J. Schafer, A. Heinrich, J. Biegert, and U. Keller, *Phys. Rev. A* **72**, 013411 (2005).
- ¹¹Z. Chang, *OSA Continuum* **2**, 2131 (2019).
- ¹²K. Murari, H. Cankaya, P. Kroetz, G. Cirimi, P. Li, A. Ruehl, I. Hartl, and F. X. Kärtner, *Opt. Lett.* **41**, 1114 (2016).
- ¹³P. Kroetz, A. Ruehl, G. Chatterjee, A.-L. Calendron, K. Murari, H. Cankaya, P. Li, F. X. Kärtner, I. Hartl, and R. J. Dwayne Miller, *Opt. Lett.* **40**, 5427 (2015).
- ¹⁴M. Hemmer, D. Sánchez, M. Jelínek, V. Smirnov, H. Jelinkova, V. Kubeček, and J. Biegert, *Opt. Lett.* **40**, 451–454 (2015).
- ¹⁵L. von Grafenstein, M. Bock, D. Ueberschaer, U. Griebner, and T. Elsaesser, *Opt. Lett.* **41**, 4668 (2016).
- ¹⁶P. Malevich, G. Andriukaitis, T. Flöry, A. J. Verhoef, A. Fernández, S. Ališauskas, A. Pugžlys, A. Baltuska, L. H. Tan, C. F. Chua, and P. B. Phua, *Opt. Lett.* **38**, 2746–2749 (2013).
- ¹⁷M. Bock, L. von Grafenstein, U. Griebner, and T. Elsaesser, *J. Opt. Soc. Am. B* **35**, C18 (2018).
- ¹⁸L. von Grafenstein, M. Bock, D. Ueberschaer, A. Koç, U. Griebner, and T. Elsaesser, *Opt. Lett.* **45**, 3836 (2020).
- ¹⁹Y. Yin, X. Ren, Y. Wang, F. Zhuang, J. Li, and Z. Chang, *Photonics Res.* **6**, 1 (2018).
- ²⁰Y. Yin, X. Ren, A. Chew, J. Li, Y. Wang, F. Zhuang, Y. Wu, and Z. Chang, *Sci. Rep.* **7**, 11097 (2017).
- ²¹Y. Yin, A. Chew, X. Ren, J. Li, Y. Wang, Y. Wu, and Z. Chang, *Sci. Rep.* **7**, 45794 (2017).